Chinese Journal of Natural Medicines

Broad-spectrum anticoronaviral activity of the traditional herbal medicine Mahuangtang by targeting the multistep viral infection process: virus entry, Mpro, PLpro, RdRp and IFN induction

Jiwon Yoon, Young-Hee Jin, Yeonhwa Kim, Eun Young Oh, Sohyun Park, Jung Sun Min, In Jin Ha, Sanghyun Kim, Hakjin Kim, Sang-Myeong Lee, Sunoh Kwon

Citation: Jiwon Yoon, Young-Hee Jin, Yeonhwa Kim, Eun Young Oh, Sohyun Park, Jung Sun Min, In Jin Ha, Sanghyun Kim, Hakjin Kim, Sang-Myeong Lee, Sunoh Kwon, Broad-spectrum anticoronaviral activity of the traditional herbal medicine Mahuangtang by targeting the multistep viral infection process: virus entry, Mpro, PLpro, RdRp and IFN induction, Chinese Journal of Natural Medicines, 2026, 24(10), 1163-1175. doi: 10.1016/S1875-5364(26)61212-5.

View online: https://doi.org/10.1016/S1875-5364(26)61212-5

Related articles that may interest you

Discovery and characterization of naturally occurring covalent inhibitors of SARS-CoV-2 M^{pro} from the antiviral herb Ephedra

Chinese Journal of Natural Medicines. 2024, 22(9), 797-807 https://doi.org/10.1016/S1875-5364(24)60577-7

Flavonoids from the roots and rhizomes of *Sophora tonkinensis* and their *in vitro* anti-SARS-CoV-2 activity

Chinese Journal of Natural Medicines. 2023, 21(1), 65-80 https://doi.org/10.1016/S1875-5364(23)60386-3

Sesquiterpenes and polyphenols with glucose-uptake stimulatory and antioxidant activities from the medicinal mushroom *Sanghuangporus sanghuang*

Chinese Journal of Natural Medicines. 2021, 19(9), 693-699 https://doi.org/10.1016/S1875-5364(21)60101-2

Scutellaria baicalensis: a promising natural source of antiviral compounds for the treatment of viral diseases

Chinese Journal of Natural Medicines. 2023, 21(8), 563-575 https://doi.org/10.1016/S1875-5364(23)60401-7

Anti-hepatitis B virus activities of natural products and their antiviral mechanisms

Chinese Journal of Natural Medicines. 2023, 21(11), 803-811 https://doi.org/10.1016/S1875-5364(23)60505-9

Probiotics with anti-type 2 diabetes mellitus properties: targets of polysaccharides from traditional Chinese medicine

Chinese Journal of Natural Medicines. 2022, 20(9), 641-655 https://doi.org/10.1016/S1875-5364(22)60210-3

Wechat

Chinese Journal of Natural Medicines 24 (2026) 1163-1175

Contents lists available at ScienceDirect

Chinese Journal of Natural Medicines

journal homepage: www.cjnmcpu.com/

Original article

Broad-spectrum anticoronaviral activity of the traditional herbal medicine Mahuangtang by targeting the multistep viral infection process: virus entry, Mpro, PLpro, RdRp and IFN induction

Jiwon Yoon[a,Δ], Young-Hee Jin[b,Δ*], Yeonhwa Kim[c], Eun Young Oh[c], Sohyun Park[c], Jung Sun Min[d], In Jin Ha[e], Sanghyun Kim[f], Hakjin Kim[g], Sang-Myeong Lee[c,*], Sunoh Kwon[d,*]

[a] *Korean Medicine Data Division, Korea Institute of Oriental Medicine, Daejeon 34054, Republic of Korea*
[b] *Korean Medicine Application Center, Korea Institute of Oriental Medicine, Daegu 41062, Republic of Korea*
[c] *College of Veterinary Medicine, Chungbuk National University, Cheongju 28644, Republic of Korea*
[d] *Korean Medicine Convergence Research Division, Korea Institute of Oriental Medicine, Daejeon 34054, Republic of Korea*
[e] *Korean Medicine Clinical Trial Center (K-CTC), Kyung Hee University Korean Medicine Hospital, Seoul 02454, Republic of Korea*
[f] *Department of Medical Classics, College of Korean Medicine, Daejeon University, Daejeon 34520, Republic of Korea*
[g] *In Quantio, Gene On Biotech, Daejeon 35229, Republic of Korea*

ARTICLE INFO

Article history:
Received 23 September 2025
Revised 13 June 2026
Accepted 15 June 2026
Available online 20 October 2026

Keywords:
Mahuangtang
Human Coronavirus
SARS-CoV-2
Mpro
PLpro
RdRp
Antivirals

ABSTRACT

Ephedra decoction, Mahuangtang (MHT), is a traditional herbal formula comprising *Ephedrae sinica* (ES), *Prunus armeniaca* (PA), *Cinnamomum cassia*(CC), and *Glycyrrhiza uralensis* (GU). MHT is used to treat colds, influenza, and other respiratory conditions. This study investigates the anticoronaviral effect of MHT and elucidates its mode of action and the active antiviral components of MHT. UHPLC-MS/MS analysis showed the holistic quality and equivalency between MHT and a mixture of four herbal components and identified nine representative compounds in MHT. The inhibitory activity of MHT and its components was examined with HCoV-OC43, SARS-CoV-2, its omicron variants, and pseudotyped lentiviruses. Time-of-addition assay, viral attachment assay, viral penetration assay, virucidal assay, and SARS-CoV-2 Mpro, PLpro, and RdRp activity assay were performed. MHT and its components, ES, CC, and GU, except PA, inhibited coronavirus infection. While MHT, and its components ES, and CC exhibited the suppression of virus entry with a virucidal activity, GU demonstrated inhibition of viral infection in the late stage. PA and its compound, amygdalin, did not inhibit coronavirus infection. Furthermore, Cinnamic aldehyde in CC and liquiritin, liquiritigenin, glycyrrhizin, and glabridin in GU were the active compounds of MHT but not ephedrine alkaloids in ES. MHT and its components inhibited the activity of Mpro and PLpro proteases and RdRp. Molecular docking analysis showed the binding affinity between RdRp and glabridin and between RBD-ACE2 and cinnamic aldehyde. Additionally, we showed that MHT induced the expression of IFN-related antiviral genes by activating the STAT1 pathway. MHT exhibited the potential to function as a multifaceted therapeutic candidate for treating broad-spectrum coronavirus infection by targeting multiple stages of viral infection.

1. Introduction

Since the COVID-19 outbreak in December 2019, human coronaviral infectious diseases have been considered a global healthcare challenge. While human coronaviruses (HCoVs), HCoV-OC43, HCoV-229E, HCoV-HKU1, and HCoV-NL63 have usually caused seasonal and mild common colds, the recently emerged SARS-CoV, MERS-CoV, and SARS-CoV-2 have caused severe respiratory diseases. HCoVs are positive single-stranded RNA viruses comprising the envelope, membrane, spike, and nucleocapsid structural proteins and the 15–16 nonstructural proteins, including main protease (Mpro, or 3CL protease) and papain-like protease (PLpro) for the proteolytic process of polyproteins, and RNA-dependent RNA polymerase (RdRp) for the viral RNA synthesis, which are crucial proteins for viral replication and serve as critical targets for viral inhibitors [1]. The Food and Drug Administration-approved COVID-19 antiviral agents, remdesivir, inhibit RdRp activity, while Paxlovid targets Mpro [2]. Although therapeutic drugs and vaccines against COVID-19 have been developed since the pandemic onset, unsolved issues persist regarding their efficacy and safety amid the continuously emerging SARS-CoV-2 variants of concern [3]. Therefore, there is a compelling need to discover new broad-spectrum anti-coronaviral therapeutic agents.

Ephedra decoction, Mahuangtang (MHT), is a traditional herbal formula that expels external pathogenic cold, known for its efficacy in inducing sweating, dispelling cold, promoting lung

* Corresponding author.
E-mail addresses: jinohee@kiom.re.kr (Y-H. Jin); smlee@chungbuk.ac.kr (S-M. Lee); sunohkwon@khu.ac.kr (S. Kwon)
Δ These authors contributed equally to this work.

https://doi.org/10.1016/S1875-5364(26)61212-5
Copyright © 2026, China Pharmaceutical University. Published by Elsevier B.V. All rights are reserved.

function, and relieving wheezing, as recorded in the *Treatise on Cold Pathogenic Diseases* (Shānghán lùn) by Zhāngzhòngjǐng in the Hàn Dynasty [4]. MHT comprises four crude drugs : Ephedra Herb, Apricot Kernel, Cinnamon Bark, and Glycyrrhiza. Their botanical origins are listed in Table 1. MHT has been widely used to treat external wind-cold patterns with symptoms such as fever, aversion to cold, body aches, headache, absence of sweat, wheezing, asthma, thin white tongue coating, and floating-tight pulses [5]. In East Asia, it is commonly used to treat respiratory infectious diseases. Recent reports have shown that MHT reduces influenza virus titers, regulates inflammatory responses, possesses antipyretic properties, and alleviates influenza virus-induced pneumonia [6-9]. MHT ameliorated asthma symptoms through its anti-inflammation mechanism in an asthma mouse model [9, 10]. In clinical studies, MHT-combined neuraminidase inhibitors proved more effective in reducing fever duration to alleviate flu symptoms and exhibited an antipyretic effect in children infected with influenza [11, 12].

Table 1 Composition of Mahuangtang (MHT).

Scientific name [Family] (abbreviation)	Crude drug name	Contents (g)	Weight ratio (%)	Compounds
Ephedra sinica Stapf [Ephedraceae] (ES)	Ephedra Herb	5.0	32.3	Ephedrine (alkaloids) Pseudoephedrine (alkaloids)
Prunus armeniaca L. [Rosaceae] (PA)	Apricot Kernel	5.0	32.3	Amygdalin (cyanoglucosides)
Cinnamomum cassia (L.) J.Presl [Lauraceae] (CC)	Cinnamon Bark	4.0	25.8	Cinnamic acid (coumarin) Cinnamic aldehyde (coumarin)
Glycyrrhiza uralensis Fisch. [Fabaceae] (GU)	Glycyrrhiza	1.5	9.6	Liquiritin (flavonoids) Liquiritigenin (flavonoids) Glycyrrhizin (triterpene saponins) Glabridin (isoflavonoid)

This study explores the effect of MHT on HCoV infections, focusing on HCoV-OC43, SARS-CoV-2, and its variants. It elucidates the active components of MHT and the mode of action in targeting various stages of the virus life cycle, host immune response, and viral proteins, including Mpro, PLpro, and RdRp, of SARS-CoV-2. These study findings reveal that MHT is a potential therapeutic candidate for treating broad-spectrum coronavirus infectious diseases.

2. Materials and methods

2.1. Reagents

MHT was kindly provided by Kracie Pharmaceutical, Ltd. (Tokyo, Japan). 1.6 g MHT was extracted at 100 °C for 3 h by adding 10 times distilled water (155 mL) to 5.0 g Ephedra Herb, 5.0 g Apricot Kernel, 4.0 g Cinnamon Bark, and 1.5 g Glycyrrhiza, centrifuged at 6000 $m \cdot s^{-2}$, concentrated under reduced pressure below 60 °C, sterilized at 120 °C, and then lyophilized. The final yield (*W*/*W*) of MHT was 10.3%.

Individual water extracts of ES, PA, CC, and GU were made by boiling 10 times (*V*/*W*) distilled water to dried crude drugs (Kwangmyungdang Pharmacy Co., Ltd., Ulsan, Korea). The reflux extraction at 94 °C for 3 h, the 53 μm pore filtration, the concentration under reduced pressure at 50 °C, and lyophilization were conducted. ES, PA, CC, and GU final yields (*W*/*W*) were 17.57%, 13.98%, 7.96%, and 24.72%, respectively. Holistic quality and equivalency analysis between MHT and the mixture of 4 herbal components (Table S1) was performed by non-targeted investigation based on chemical profiles as fingerprints using Ultra-High-Performance Liquid Chromatography-Tandem Mass Spectrometry (UHPLC-MS/MS) coupled with correlation analysis as described in supplementary methods. The Pearson correlation coefficient was > 0.9 (Fig. S1, Tables S2 and S3). Ephedrine HCl (PubChem CID: 65326, ≥ 99.96% purity) and pseudoephedrine HCl (PubChem CID: 9581, ≥ 99.95% purity) were obtained from the National Institute of Food and Drug Safety Evaluation (Cheongju, Korea). ChemFaces Biochemical Co., Ltd. (Wuhan, China) supplied amygdalin (PubChem CID: 656516), cinnamic acid (PubChem CID: 444539), cinnamic aldehyde (PubChem CID: 637511), liquiritin (PubChem CID: 503737), liquiritigenin (PubChem CID: 114829), glycyrrhizin (PubChem CID: 14982), and glabridin (PubChem CID: 124052), each with purity of ≥ 98%. These compounds were prepared and stored as 100 $mmol \cdot L^{-1}$ solutions in DMSO (Sigma-Aldrich, St. Louis, MO, USA) at −80 °C.

2.2. Cells and viruses

MRC-5 (ATCC, Manassas, VA, USA) and A549-hACE2-TMPRSS2 cells (InvivoGen, San Diego, CA, USA) were cultured in MEM (Corning, NY, USA) with 10% FBS (Thermo Fisher Scientific, Sunnyvale, CA) and 1% penicillin/streptomycin (PS; Thermo). Vero E6 cell (ATCC) and HEK293T cell (ATCC) were cultured in DMEM (Corning) with 10% FBS and 1% PS. HCoV-OC43 (ATCC) was propagated, titrated, and infected in MRC-5 cells as previously described [13]. Pseudovirus expressing EGFP and VSV-G envelope, or Spike protein (S) of SARS-CoV-2 variants (501Y.V2, B.1.617.2, and B.1.617.2.1 variant) were obtained from VectorBuilder Inc. (Guangzhou, China). The SARS-CoV-2 strains (NCCP 43326: S Clade, NCCP 43412: GRA Clade omicron BA.2, NCCP 43417: GRA Clade omicron BA.2.75, NCCP 43425: GRA Clade omicron BA.4, NCCP 43426: GRA Clade omicron BA.5) were gifted by the National Culture Collection for Pathogens (NCCP, Cheongju, Korea). SARS-CoV-2 was amplified, titrated, and infected in Vero E6 cells as previously described [14, 15].

2.3. Viral cytopathic effect (CPE) reduction assay

HCoV-OC43-infected MRC-5 cells (1×10^4 cells/96-well plate) were incubated for 4 d. A colorimetric compound, 3-(4,5-dimethylthiazol-2-yl)-5-(3-carboxymethoxyphenyl)-2-(4-sulfophenyl)-2*H*-tetrazolium, inner salt (MTS, Promega Corporation, Madison, WI, USA) was administered into culture media, and the optical density at 490 nm was detected after 2 h with a GloMax® Microplate Reader (Promega Corporation). After a 2-day incubation of SARS-CoV-2-infected Vero E6 cells, cells were fixed with 4% formaldehyde solution, stained with 0.4% crystal violet solution, and then treated with a solubilization solution (Sigma). Absorbance at 550 nm was measured.

2.4. Quantitative reverse transcription polymerase chain reaction (qRT-PCR)

The total RNAs of the infected cells extracted by the RNeasy® Mini Kit (Qiagen N.V., Hilden, Germany), or the extracellular RNAs of the culture supernatant collected by a QIAamp viral RNA mini kit (Qiagen), and the primers for the HCoV-OC43 nucleocapsid protein (N) (5′-AGCAACCAGGCTGATGTCAATACC-3′ and 5′-AGCAGACCT TCCTGAGCCTTCAAT), or SARS-COV-2 receptor binding domain (RBD, 5′-CAATGGTTTAACAGGCACAGG-3′ and 5′-CTCAAGTGTCTGTGGATCACG) were reacted in the One Step TB Green® PrimeScript™ RT-PCR kits (Takara Bio Inc., Kusatsu, Ja-

pan) using CFX Opus 96 Real-time PCR (Bio-Rad Lab., Hercules, CA, USA). Serially diluted HCoV-OC43 N or SARS-CoV-2 RBD standards (10^1–10^{10} copies/μL) were employed to calculate viral RNA copy numbers. The primers for interferon-alpha 1 (*IFNA1*), interferon-beta 1 (*IFNB1*), interferon-lambda 1 (*IFNL1*), myxovirus resistance protein 1 (*MX1*), and beta-actin (*ACTB*) have been described previously [13].

2.5. Immunofluorescence staining

4% paraformaldehyde fixation solution and 0.2% Triton X-100 permeabilization solution were used. After blocking, cells were reacted with the anti-HCoV-OC43 S antibody (Ab) (CusaBio, Houston, TX, USA), anti-HCoV-OC43 N Ab (Merck & Co., Inc. Rahway, NJ, USA), or anti-SARS-CoV-2 N Ab (Sino Biological Inc., Beijing, China), and then reacted with the AlexaFluor488 or 555-conjugated secondary Ab (Thermo Fisher), followed by mounting with SlowFade™ Gold Antifade Mountant with DAPI (Thermo Fisher). The cells were visualized using a fluorescence microscope and CellSens Dimension software (Olympus, Tokyo, Japan).

2.6. Western blot analysis

The proteins of cell lysates were separated by SDS-PAGE and transferred to membranes, followed by blocking with EveryBlot blocking buffer (Bio-Rad Lab). The anti-HCoV-OC43 S Ab (CusaBio), anti-HCoV-OC43 N Ab (Merck & Co., Inc.), anti-total Signal transducer and activator of transcription 1 (STAT1) Ab (Cell Signaling Technology, Danvers, MA, USA), anti-phospho-STAT1 Ab (Cell Signaling Technology), or anti-β-actin Ab (Cell Signaling Technology) was incubated, and then the HRP-conjugated secondary Ab was incubated. Chemidoc™ MP Gel Imaging System and ImageLab program (Bio-Rad) were used to detect and quantify the proteins.

2.7. Time-of-Addition assay

To assess pretreatment effects against HCoV-OC43 infection, MRC-5 cells were exposed to MHT for 24 h before virus inoculation, followed by washing and subsequent viral infection. For the cotreatment assay, MHT was simultaneously treated with the virus for 4 h, followed by cell washing. For the posttreatment assay, cells were initially infected with the virus, 4 h after which MHT was added. At 4 dpi, the CPE reduction assay was conducted. For SARS-CoV-2 infection experiments, Vero E6 cells were treated with MHT for 1 h before, during infection for 1 h, or at 1 h after infection, and a plaque reduction assay was subsequently conducted at 2 dpi, as described below.

2.8. Viral attachment assay, viral penetration assay, and virucidal assay

MRC-5 cells were pre-incubated with HCoV-OC43 and MHT at 4 °C for 1 h and subsequently washed and incubated for 24 h for the attachment assay. In the penetration assay, the HCoV-OC43 virus was added to pre-chilled cells at 4 °C for 1 h to render virus attachment. The cells were washed and treated with MHT at 33 °C for 1 h, followed by further washing and incubation at 33 °C for 23 h. For the virucidal assay, the virus was pretreated with MHT for 1 h at 4 °C, after which the cells were infected with the pretreated virus and MHT mixture at 33 °C for 1 h. The cells were finally washed and incubated for an additional 23 h, followed by harvesting for viral RNA copy number analysis.

2.9. Plaque reduction assay

The Vero E6 cells were infected with 0.01 MOI SARS-CoV-2 for 1 h. Then cells were washed, overlaid with 0.5% agarose media, and incubated for 48 h. The 4% formaldehyde solution was used for cell fixation, and the 0.4% crystal violet solution was used for cell staining.

2.10. Pseudovirus infection assay

Pseudotyped lentiviruses (10 MOI) were introduced into A549-hACE2-TMPRSS2 cells with MHT for 4 h at 33 °C. Subsequently, the cells were incubated for 68 h. The images were photographed by a fluorescence microscope (Olympus Corporation, Tokyo, Japan), and the fluorescence intensity was detected using FACS (LSRFortessa X-20, BD Biosciences, San Jose, CA, USA).

2.11. UHPLC-MS/MS analysis

The holistic quality and equivalency analysis between MHT and 4 components mixture (Table S1) was performed by non-targeted investigation based on chemical profiles as fingerprints using UHPLC-QTOF-MS/MS coupled with correlation analysis as described in supplementary methods. The UHPLC-MS/MS analysis using the Thermo Scientific Vanquish UHPLC system hyphenated with a 3200 QTRAP mass spectrometer system (SCIEX, Foster City, CA, USA) was conducted to quantify the nine chemical markers in MHT as described in the supplementary methods.

2.12. SARS-CoV-2 Mpro assay and PLpro assay

Mpro (SARS-CoV-2) assay kits (BPS Bioscience, San Diego, CA, USA) and PLpro (SARS-CoV-2) assay kits (BPS Bioscience) were used to measure the viral protease activity following the manufacturer's instructions. The fluorescence intensity at 360 nm/460 nm excitation/emission wavelengths was detected with a SpectraMax® iD5 microplate reader (Molecular Devices, San Jose, CA, USA).

2.13. Cell-Based SARS-CoV-2 RdRp activity assay

HEK293T cells were co-transfected with the nsp12 expression plasmid, pCI-SARS-CoV-2 nsp12, and the reporter plasmid, p(+)FLuc-(−)UTR-NLuc with transIT®-LT1 transfection reagent (Mirus Bio LLC., Madison, WI, USA). After 24 h, the expression ratio of firefly luciferase and nano luciferase was determined with the Nano-Glo® Dual-Luciferase® Reporter Assay System (Promega) and GloMax® Microplate Reader (Promega), as previously described [16].

2.14. Molecular docking analysis

Binding features between RdRp (PDB ID: 7BV2, resolution: 2.50 Å) and remdesivir triphosphate (RTP; ligand ID: F86) or glabridin were analyzed. Non-essential ligands/ions were removed while preserving the catalytic pocket, including the NTP entry channel, using PyMOL (Schrödinger LLC, New York, USA). To analyze binding between the SARS-CoV-2 RBD-ACE2 complex (PDB ID: 6M0J, resolution: 2.45 Å) and cinnamic aldehyde, the crystal structure was converted to PDBQT format containing both ACE2 (chain A, 614 residues) and RBD (chain E, 193 residues), and cinnamic aldehyde was energy-minimized using Open Babel and converted to PDBQT format using AutoDockTools. Docking was carried out using AutoDock Vina [17] with the following parameters: exhaustiveness = 16, number of modes = 20, and energy range = 4 kcal·mol^{-1} for RdRp, and with the following parameters: exhaustiveness = 32, number of modes = 20, energy range = 4 kcal·mol^{-1} for RBD-ACE2 complex.

2.15. Statistical analysis

Statistical analysis was conducted using GraphPad Prism Software V.10.4.1 (GraphPad Software, Inc., San Diego, CA, USA). Data were expressed as mean ± standard error of the mean (SEM). Probability (*P*) values were obtained through one-way analysis of variance (ANOVA), followed by Bonferroni's post hoc test ($^{*}P < 0.05$, $^{**}P < 0.01$, $^{***}P < 0.001$ and $^{****}P < 0.0001$ *vs* Control).

3. Results

3.1. MHT inhibited the infection of HCoV-OC43, SARS-CoV-2, and omicron variants

To evaluate the antiviral efficacy of MHT, MRC-5 cells were incubated with MHT for 48 h during infection, and the HCoV-OC43-induced CPE was determined using the MTS assay at 4 dpi (Fig. 1A). MHT exhibited protection against HCoV-OC43-induced CPEs, with 233.57 μg·mL^{-1} IC_{50} and a selectivity index (SI, CC_{50}/IC_{50}) of > 4.3 (Fig. 1B). To examine the MHT effect on virus replication, the viral RNA copy numbers were quantified in virus-infected MRC-5 cell lysates (intracellular) and supernatants (extracellular) treated with MHT (500, 750, and 1000 μg·mL^{-1}) using qRT-PCR at 1 and 2 dpi. Compared with the viral RNA copy numbers of virus-infected cells, MHT treatment led to a reduction in the intracellular and extracellular viral RNA copy numbers at 1 and 2 dpi (Fig. 1C). Immunofluorescence staining analysis revealed the decreased levels of S and N in MHT-treated cells at 2 dpi (Fig. 1D). Western blot analysis was performed to confirm the decreased expression level of viral proteins, revealing a dose-dependent reduction in the levels of S (145 kDa) and N (50.4 kDa) expression by MHT at 2 dpi (Fig. 1E). Collectively, these data suggest that MHT exhibits anti-HCoV-OC43 activity by protecting against virus-induced CPE and inhibiting viral replication and the expression level of viral proteins.

We examined whether MHT inhibited SARS-CoV-2 infection. MHT markedly reduced SARS-CoV-2-induced CPE, with an IC_{50} value of 88.95 μg·mL^{-1} and a CC_{50} > 2000 μg·mL^{-1} (SI > 22.5) (Fig. 2A and Supplementary Figure S2A). Upon detection of viral RNA copy numbers and the expression level of viral N subsequent to treatment with MHT *via* qRT-PCR and immunofluorescence staining, respectively, a significant reduction in viral RNA levels (Fig. 2B) and N expression (Figs. 2C and 2D) was observed at 500 μg·mL^{-1}. Examination of the antiviral activity of MHT against newly emerging omicron variants of SARS-CoV-2—BA.2, BA.2.75, BA.4, and BA.5—revealed its efficacy in reducing their CPEs (Fig. 2E) and its dose-dependent decreasing effects on the level of N expression in these omicron variant-infected Vero E6 cells (Figs. 2F and 2G). Overall, the MHT suppressing effect on the infection of HCoV-OC43, SARS-CoV-2, and its omicron variants suggests its potential as a broad-spectrum anticoronaviral inhibitor.

3.2. MHT exhibited the inhibition of virus entry with a virucidal effect

A time-of-addition assay was conducted to clarify at which stage of virus infection MHT exerts its antiviral activity (Fig. 3A). MHT cotreatment, even for 4 h, protected the virus-induced CPE, but pretreatment and posttreatment of MHT could not (Fig. 3B). These data imply that MHT effectively disrupts the early stages. Viral attachment assay and viral penetration assay were conducted to identify the specific target stage, revealing that MHT demonstrated significant dose-dependent suppression of virus attachment and penetration (Figs. 3C and 3D). MHT itself also ex-

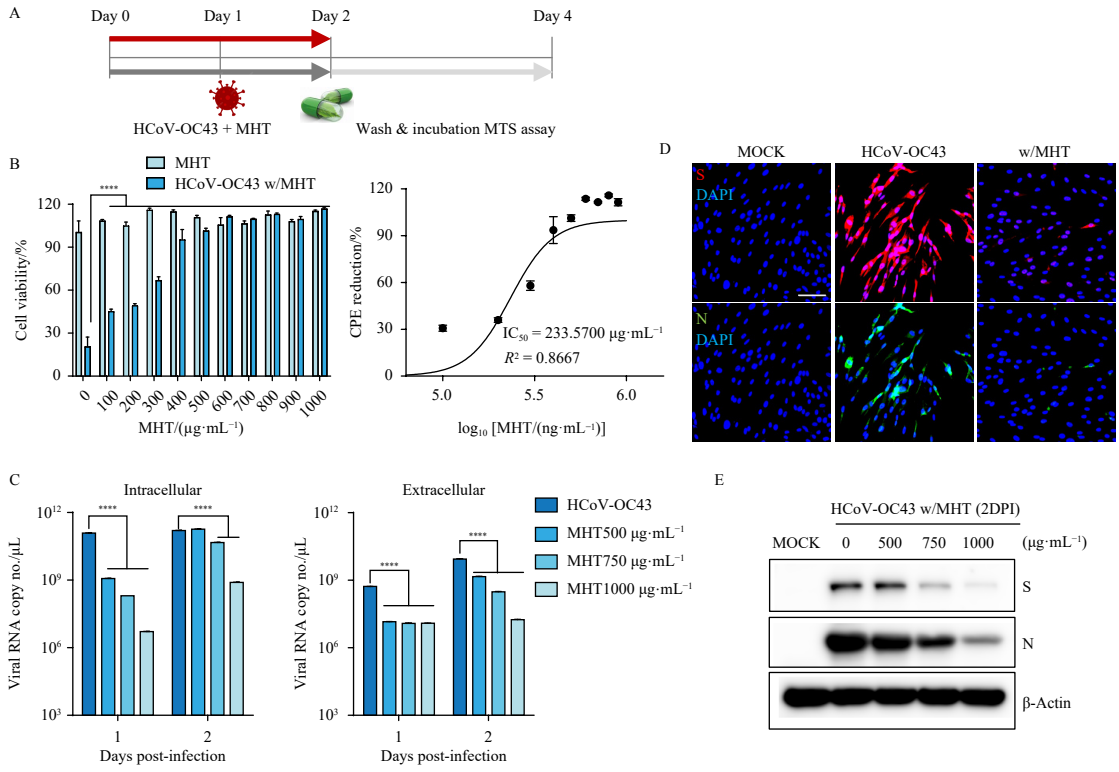


Fig. 1 Mahuangtang (MHT) inhibited HCoV-OC43 infection in MRC-5 cells. (A) Scheme for the HCoV-OC43 infection experiment. (B) HCoV-OC43-induced cytopathic effect (CPE) under MHT treatment using MTS at 4 days postinfection (dpi). Data were analyzed using one-way ANOVA, followed by Bonferroni's multiple comparisons test ($F_{10,22}$ = 345.8, $P < 0.0001$). The IC_{50} of MHT was 233.57 μg·mL^{-1} based on nonlinear regression analysis. (C) Intracellular and extracellular viral RNA levels in virus-infected cells treated with MHT were determined using qRT-PCR at 1 and 2 dpi. Data were analyzed using one-way ANOVA, followed by Bonferroni's multiple comparisons test (intracellular 1 dpi: $F_{3,4}$ = 51409, $P < 0.0001$; intracellular 2 dpi: $F_{3,4}$ = 18947, $P < 0.0001$; extracellular 1 dpi: $F_{3,4}$ = 2863, $P < 0.0001$; extracellular 2 dpi: $F_{3,4}$ = 5578, $P < 0.0001$). (D) Expression of HCoV-OC43 spike protein (S) (red, upper panel) and nucleocapsid protein (N) (green, lower panel) and nucleus (blue, DAPI) visualized by immunofluorescence staining at 2 dpi (200 × magnification; Scale bar = 100 μm). (E) Expression of viral S and N in HCoV-OC43-infected MRC-5 cells treated with MHT at 2 dpi by Western blot analysis. The β-actin was detected as a control. Data were represented as mean ± SEM of three independent experiments.

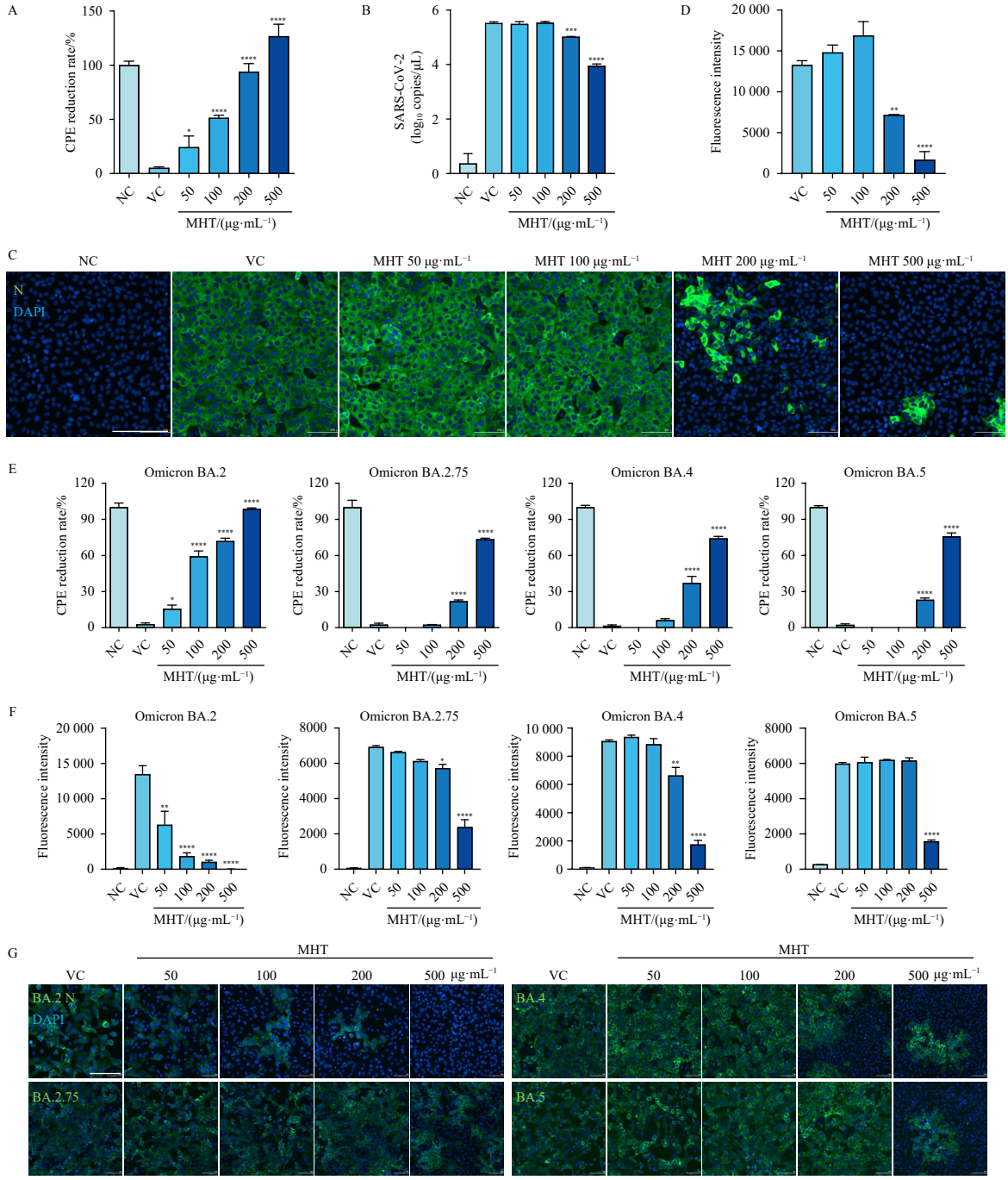


Fig. 2 MHT suppressed SARS-CoV-2 and its omicron variant infections. (A) SARS-CoV-2-infected Vero E6 cells were treated with MHT, and the cytopathic effect (CPE) reduction rate was determined with crystal violet staining at 2 dpi. NC, normal control, VC, virus infection control. Data were analyzed using one-way ANOVA, followed by Bonferroni's multiple comparisons test ($F_{4,10}$ = 126.8, P < 0.0001). (B) The viral RNA copy number of SARS-COV-2-infected Vero E6 cells with MHT was detected with qRT-PCR ($F_{4,10}$ = 132.7, P < 0.0001). (C and D) N (green) and nucleus (DAPI, blue) detected in SARS-CoV-2-infected and MHT-treated Vero E6 cells by immunofluorescence staining (C) and fluorescence intensity of N (D). Data were analyzed by one-way ANOVA with Bonferroni's multiple comparisons test ($F_{4,10}$ = 38.36, P < 0.0001). (E) SARS-CoV-2 omicron variants, BA.2, BA.2.75, BA.4, and BA.5, were inoculated into Vero E6 cells under MHT treatment, and the CPE reduction assay was conducted at 2 dpi. (F and G) Vero E6 cells infected with omicron variants under MHT treatment and N (green) with nucleus (DAPI, blue) detected by immunofluorescence staining (100 × magnification; Scale bar = 200 μm). The fluorescence intensity of N was measured using ImageJ. Data were represented as mean ± SEM of three independent experiments and analyzed using one-way ANOVA, followed by Bonferroni's multiple comparisons test (BA.2: $F_{4,10}$ = 27.95, P < 0.0001; BA2.75: $F_{4,10}$ = 66.58, P < 0.0001; BA.4: $F_{4,10}$ = 80.91, P < 0.0001; BA.5: $F_{4,10}$ = 168.3, P < 0.0001). Data were representative of at least three independent experiments.

hibited virucidal activity. Overall, these results indicate that MHT possesses antiviral efficacy against HCoV-OC43 by inhibiting virus entry and exerting a virucidal effect.

In the time-of-addition assay with SARS-CoV-2 infection, cotreatment with 100 μg·mL^{-1} MHT completely blocked SARS-CoV-2-induced plaque formation, while 500 μg·mL^{-1} MHT pretreatment and posttreatment completely inhibited plaque formation. This suggests that the optimal working time of MHT was cotreatment, consistent with the findings for HCoV-OC43 (Fig. 3E).

We further evaluated the effect of MHT on the infection of SARS-CoV-2-pseudotyped lentivirus carrying GFP and variants S, including the 501Y.V2 South Africa variant, B.1.617.2 delta variant, or B.1.617.2.1 delta plus variant. Upon infecting A549-hACE2-TMPRSS2 cells with 10 MOI pseudotyped lentivirus and MHT treatment, we observed the inhibition—independent of viral envelope protein—of lentivirus infection, as evidenced by the level of GFP expression at 3 dpi. Data suggest that MHT effectively suppressed pseudotyped lentivirus infection irrespective of the viral envelope protein (Fig. 3F and Supplementary Figure S3). Therefore, MHT inhibits coronavirus infection by blocking virus entry

at the early stage of its life cycle.

3.3. Antiviral active herbal components of MHT

To elucidate the antiviral activity of individual herbal components of MHT—ES, PA, CC, and GU—against HCoV-OC43 infection, MRC-5 cells were treated with extracts of each herb at 100–1000 μg·mL^{-1} for 4 (Fig. 4A) or 96 h (Fig. 4B). Although ES had a CC_{50} of 241 μg·mL^{-1}, a partial CPE reduction at 100 and 200 μg·mL^{-1} concentrations with up to 60% cell viability was ob-

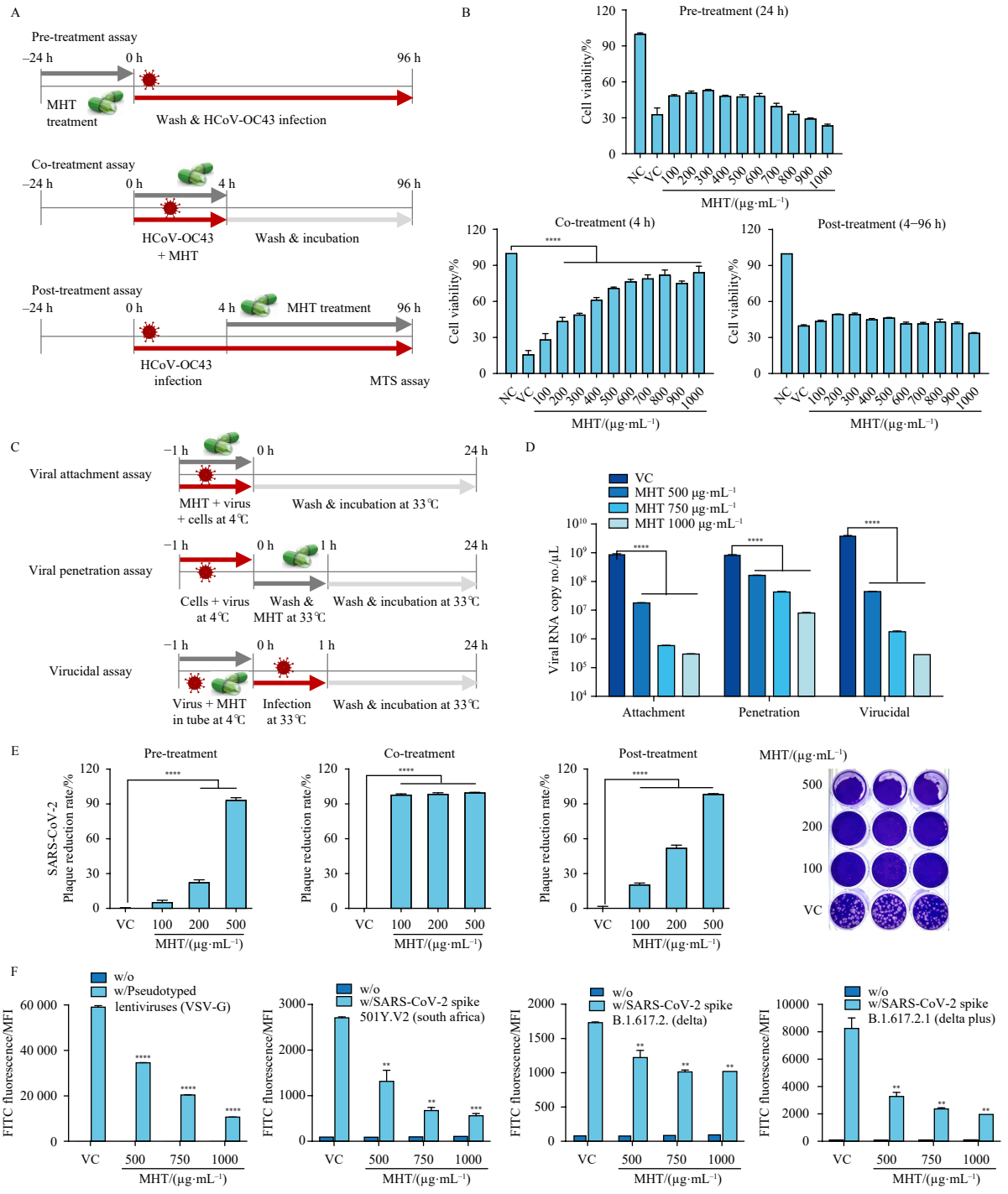


Fig. 3 MHT inhibited coronavirus infection by impeding the virus entry stage. (A) Scheme for the time-of-additional assay. (B) MRC-5 cells were incubated with MHT for 24 h prior to viral infection (pretreatment 24 h), for 4 h with infection (cotreatment 4 h), or 4 h post infection (posttreatment 4–96 h), and CPE reduction was analyzed by MTS-based assay at 4 dpi. NC, normal control; VC, viral infection control. Data were analyzed using one-way ANOVA, followed by Bonferroni's multiple comparisons test (co-treatment 4 h: $F_{10,22} = 55.07$, $P < 0.0001$). (C) Scheme of the viral attachment assay, the viral penetration assay, and the virucidal assay. (D) The viral RNA level was determined by qRT-PCR at 1 dpi after each assay. Data were analyzed using one-way ANOVA, followed by Bonferroni's multiple comparisons test (Attachment: $F_{3,4} = 319.3$, $P < 0.0001$; Penetration: $F_{3,4} = 2307$, $P < 0.0001$; Virucidal: $F_{3,4} = 1307$, $P < 0.0001$). (E) Time-of-addition assay with SARS-CoV-2 and MHT treatment. Pretreatment, cotreatment, and posttreatment of MHT in SARS-COV-2-infected Vero E6 cells and plaque reduction assay were conducted at 2 dpi. The plaque reduction assay plate was photographed. Data were analyzed using one-way ANOVA, followed by Bonferroni's multiple comparisons test (Pre-treatment: $F_{3,8} = 587.2$, $P < 0.0001$; Co-treatment: $F_{3,4} = 2403$, $P < 0.0001$; Post-treatment: $F_{3,4} = 637.7$, $P < 0.0001$). (F) The infection of pseudotyped lentivirus expressing EGFP with VSV-G envelope protein (VSV-G), 501Y.V2 variant S (South Africa), B.1.617.2. variant S (Delta), or B.1.617.2.1 variant S (Delta plus) was evaluated under MHT treatment. A549-hACE2-TMPRSS2 cells were determined with the fluorescence intensity (MFI) of GFP using FACS. Data were analyzed using one-way ANOVA, followed by Bonferroni's multiple comparisons test (VSV-G: $F_{3,4} = 4270$, $P < 0.0001$; 501Y.V2: $F_{3,4} = 58.45$, $P = 0.0009$; B.1.617.2: $F_{3,4} = 38.85$, $P = 0.0020$; B.1.617.2.1: $F_{3,4} = 49.53$, $P = 0.0013$). Data were representative of at least three independent experiments.

served, suggesting its anti-HCoV-OC43 activity. PA exhibited no CPE reduction. CC showed a 100% CPE reduction at 500 μg·mL^{-1} for 4 h incubation with an IC_{50} of 165.8 μg·mL^{-1}, suggesting its antiviral activity in the early stage, but 96 h incubation with CC showed cytotoxicity with a CC_{50} of 908.62 μg·mL^{-1}, and it still exhibited a CPE reduction with up to 400 μg·mL^{-1} CC. GU treatment did not show any cytotoxicity up to 1000 μg·mL^{-1}, and only 96 h incubation with GU protected from the HCoV-OC43-induced CPE with 622.3 μg·mL^{-1} IC_{50}, suggesting its antiviral activity in the late stage of the virus life cycle. These data indicate that ES, CC, and GU, except for PA, mainly contribute to MHT antiviral activity. Since MHT suppressed virus entry, we also performed the viral attachment, penetration, and virucidal assays using the four herbal components (Fig. 4C). Among the antiviral components, ES and CC inhibited viral attachment and penetration and exhibited virucidal activity, but GU did not inhibit virus entry, consistent with previous findings for the CPE reduction assay for 4 h (Fig. 4A).

To identify the antiviral active herbal component against SARS-CoV-2, each herbal component was administered to SARS-CoV-2-infected Vero E6 cells. ES, CC, and GU, except PA, reduced SARS-CoV-2-induced CPE with IC_{50} values of 166.4, 145.5, and 228.2 μg·mL^{-1}, respectively, and CC_{50} > 500 μg·mL^{-1} (Fig. 4D and Supplementary Figure S2B), consistent with the findings obtained for the antiviral components against HCoV-OC43.

To further define the antiviral active compounds of MHT, nine major compounds were identified based on LC-MS/MS analysis under mass parameters (Table S4). We verified that MHT comprised nine representative compounds, including cinnamic aldehyde, glycyrrhizin, liquiritin, glabridin, liquiritigenin, cin-

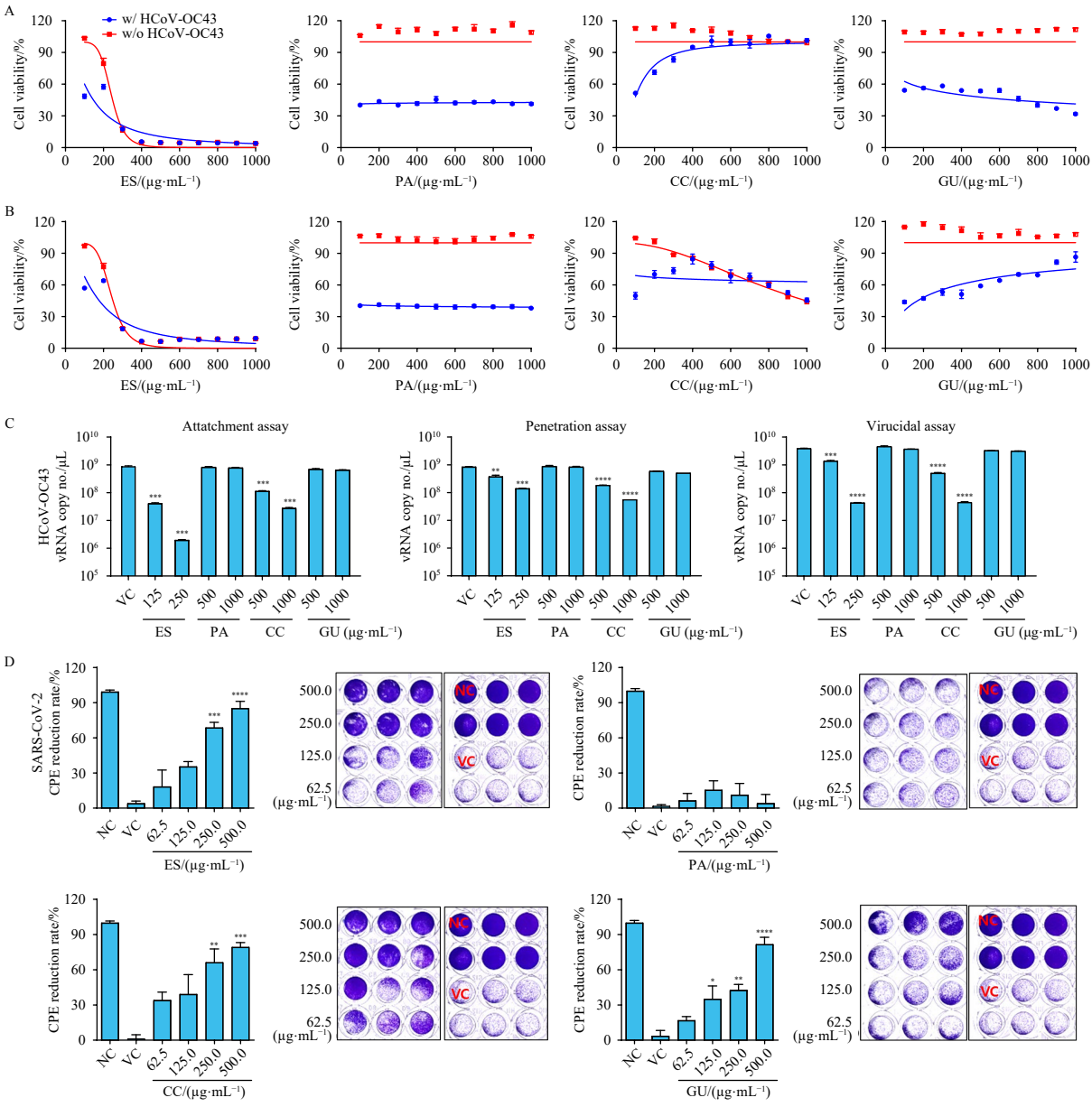


Fig. 4 Antiviral active herbal components of MHT. (A and B) CPE induced by HCoV-OC43 infection was detected with treatment of MHT herbal components, *Ephedra sinica* (ES), *Prunus armeniaca* (PA), *Cinnamomum cassia* (CC), and *Glycyrrhiza uralensis* (GU) for 4 h (A) or 96 h (B) using an MTS assay at 4 dpi. (C) Viral attachment, viral penetration, and virucidal assays of the MHT herbal component, ES, PA, CC, and GU, were conducted, and the viral RNA level was measured by qRT-PCR at 1 dpi. Data were analyzed using one-way ANOVA, followed by Bonferroni's multiple comparisons test (Attachment ES: $F_{2,3}$ = 308.0, P = 0.0003; Attachment CC: $F_{2,3}$ = 273.1, P = 0.0004; Penetration ES: $F_{2,3}$ = 155.6, P = 0.0009; Penetration CC: $F_{2,3}$ = 2127, P < 0.0001; Virucidal ES: $F_{2,3}$ = 723.4, P < 0.0001; Virucidal CC: $F_{2,3}$ = 1101, P < 0.0001). (D) SARS-CoV-2-induced CPE reduction under treatment with MHT herbal components, ES, PA, CC, and GU, was determined using the crystal violet staining at 48 h. Data were analyzed using one-way ANOVA, followed by Bonferroni's multiple comparisons test (ES: $F_{4,10}$ = 20.56, P < 0.0001; CC: $F_{4,10}$ = 9.466, P = 0.0020; GU: $F_{4,10}$ = 20.42, P < 0.0001). Data were representative of at least three independent experiments.

namic acid, amygdalin, L-ephedrine, and D-pseudoephedrine (Figs. 5A and 5B). The chemical information and contents of these nine compounds of MHT are described in Fig. 5C and Table S5.

To examine the antiviral activity of these compounds against HCoV-OC43, each compound was administered to HCoV-OC43-infected MRC-5 cells, and the viral copy numbers were determined at 1 dpi (Fig. 5D). L-ephedrine and D-pseudoephedrine in ES and amygdalin in PA could not reduce viral RNA levels. Cinnamic al-

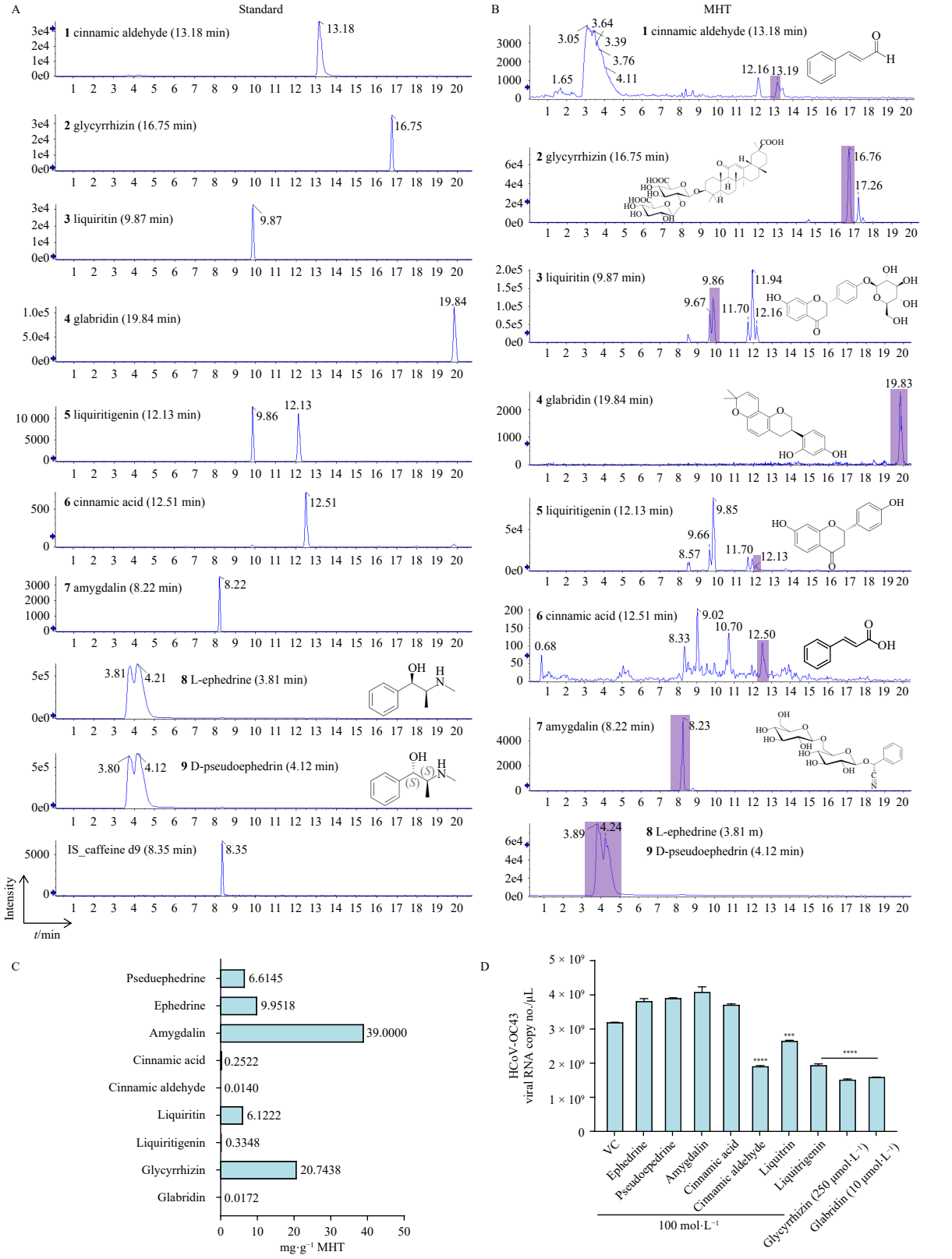


Fig. 5 Antiviral active compounds of MHT. (A and B) Representative extracted ion chromatograms of standard compounds (A) and each compound in MHT (B), and chemical structures of compounds. (C) Contents of individual compounds presented in MHT were calculated by LC-MS/MS. (D) The viral RNA level was detected in virus-infected MRC-5 cells with each compound treatment at 1 dpi by qRT-PCR. Data were representative of three independent experiments and analyzed using one-way ANOVA, followed by Bonferroni's multiple comparisons test ($F_{9,10}$ = 294.3, P < 0.0001).

dehyde, but not cinnamic acid, in CC could decrease the viral RNA level. Liquiritin, liquiritigenin, glycyrrhizin (at 250 μmol·L^{-1}), and glabridin (at 10 μmol·L^{-1}) in GU reduced the viral RNA level with no cytotoxicity (Supplementary Figure S2C).

These data indicate that ES, CC, and GU, except PA, among the MHT components inhibited coronavirus infections. Furthermore, ES and CC inhibited the virus entry, and GU exhibited suppression of virus infection in the late stage of the virus life cycle. PA lacked antiviral activity. Moreover, cinnamic aldehyde in CC, and liquiritin, liquiritigenin, glycyrrhizin, and glabridin in GU mainly contribute to the antiviral activity of MHT against HCoV-OC43.

3.4. MHT inhibited the activity of viral proteins—Mpro, PLpro, and RdRp

To further elucidate the viral target proteins of MHT, we measured the activity of three main viral proteins of SARS-CoV-2—Mpro, PLpro, and RdRp—upon MHT treatment. In the viral protease activity assay, MHT dose-dependently inhibited the activity of Mpro and PLpro, although it more efficiently inhibited the activity of PLpro than that of Mpro (Figs. 6A and 6B). Among the compounds of MHT, cinnamic aldehyde in CC and liquiritigenin and glabridin in GU inhibited the activity of Mpro and PLpro, and glycyrrhizin in GU slightly inhibited Mpro activity but not PLpro activity (Figs. 6C and 6D).

To detect the effect of MHT on the activity of SARS-CoV-2 RdRp, a cell-based SARS-CoV-2 RdRp assay system was tested, as previously published [16]. MHT dose-dependently inhibited the activity of RdRp detected by nano-luciferase (reporter signal) and firefly-luciferase activities (internal control signal) with an IC_{50} of 352.16 ± 40.28 μg·mL^{-1} (Fig. 6E). Moreover, among the herbal components, GU most strongly inhibited the RdRp activity of SARS-CoV-2 up to 70% at 800 μg·mL^{-1}, but ES and CC inhibited only around 30%, and PA could not at all (Fig. 6F). Therefore, we further determined the effect of GU compounds on SARS-CoV-2 RdRp activity and found that glycyrrhizin, liquiritin, liquiritigenin, and glabridin in GU all dose-dependently inhibited the activity of RdRp, with IC_{50} values of 67.5, 23.0, 21.3, and 7.25 μg·mL^{-1}, respectively, without cytotoxicity. Cinnamic aldehyde, in CC, could not inhibit RdRp activity (Fig. 6G and Supplementary Figure S2D). These data suggest that MHT and its compounds can efficiently inhibit the activity of viral proteins, including Mpro, PLpro, and RdRp of SARS-CoV-2, acting as direct-acting antivirals.

3.5. Molecular docking analysis

To reinforce the inhibition of RdRp activity by glabridin, we further evaluated the binding potential of glabridin with a constraint-based docking analysis, focusing the grid on experimentally validated residues (Asp623, Asn691, and Ser759) of the RdRp functional pocket (NTP-binding sites). Remdesivir triphos-

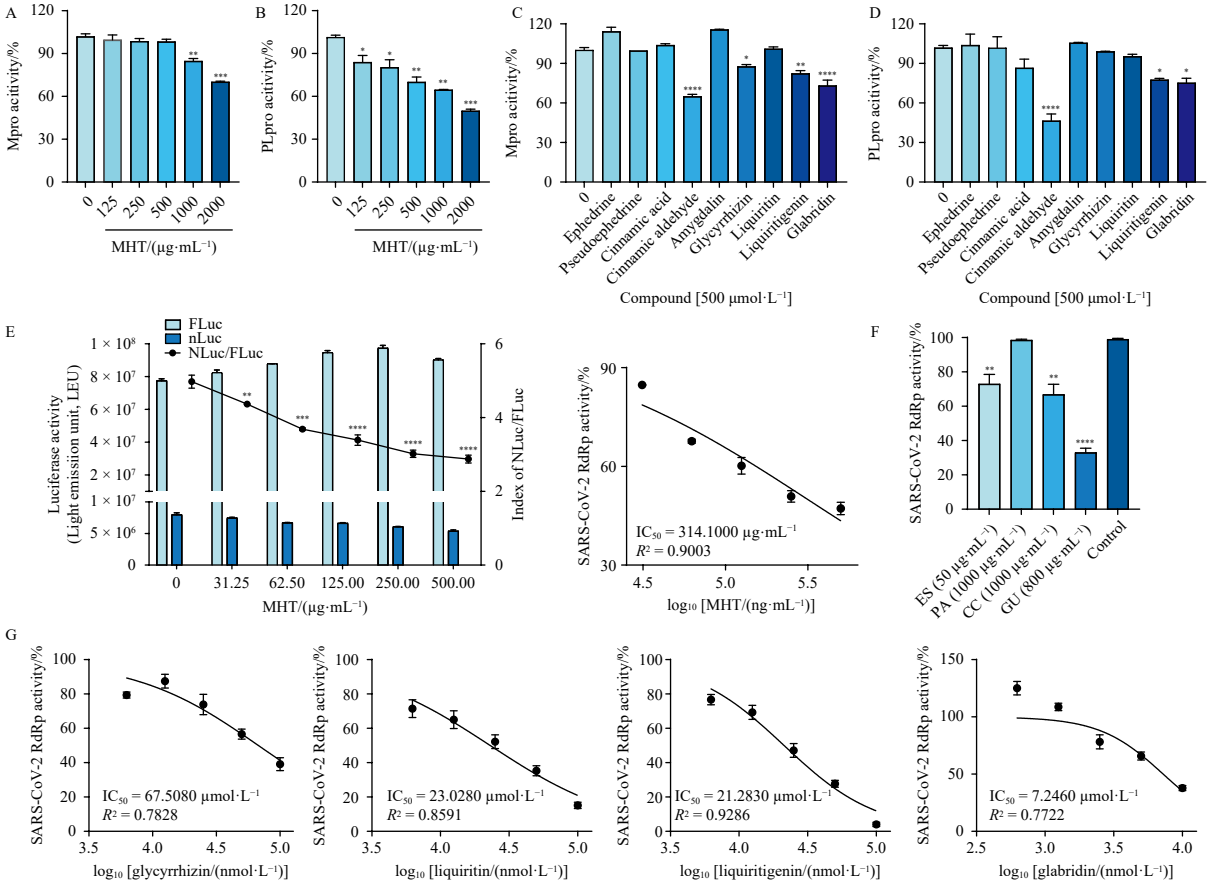


Fig. 6 MHT inhibited the activity of SARS-CoV-2 proteases, main protease (Mpro) and papain-like protease (PLpro), and RNA-dependent RNA polymerase (RdRp) activity. (A and C) Mpro activity under MHT treatment (125–2000 μg·mL^{-1}) (A) and its nine compounds treatment (500 μmol·L^{-1}) (C) was determined by SARS-CoV-2 Mpro assay. Data were analyzed using one-way ANOVA, followed by Bonferroni's multiple comparisons test (MHT: $F_{5,6}$ = 35.85, P = 0.0002; 9 compounds: $F_{9,10}$ = 64.40, P < 0.0001). (B and D) PLpro activity under the treatment of a serially diluted MHT (125–2000 μg·mL^{-1}) (B) and its nine compounds treatment (500 μmol·L^{-1}) (D) was determined using the SARS-CoV-2 PLpro assay. Data were analyzed using one-way ANOVA, followed by Bonferroni's multiple comparisons test (MHT: $F_{5,6}$ = 28.81, P = 0.0004; 9 compounds: $F_{9,10}$ = 14.99, P = 0.0001). (E) The activity of firefly-luciferase (FLuc) as an internal control and nano-luciferase (NLuc) was measured using the cell-based SARS-CoV-2 RdRp assay under MHT treatment (62.5–500 μg·mL^{-1}), and the NLuc/FLuc ratio was graphed as RdRp activity (left graph). Data were analyzed using one-way ANOVA, followed by Bonferroni's multiple comparisons test ($F_{4,15}$ = 18.19, P < 0.0001). The IC_{50} value of MHT was calculated through nonlinear regression analysis (right graph). (F) SARS-CoV-2 RdRp activity was determined with the indicated concentration of four herbal components of MHT: ES, PA, CC, and GU. Data were analyzed using one-way ANOVA, followed by Bonferroni's multiple comparisons test ($F_{4,6}$ = 66.10, $^{**}P$ < 0.01 and $^{***}P$ < 0.001 *vs* Control). (G) RdRp activity and IC_{50} value under treatment with glycyrrhizin, liquiritin, liquiritigenin, and glabridin based on the cell-based SARS-CoV-2 RdRp assay. Data were representative of at least three independent experiments.

phate (RTP), the active form of remdesivir, competes with endogenous nucleotides in the RdRp of SARS-CoV-2, known as an RdRp inhibitor. In silico docking analysis showed that both glabridin and RTP were confirmed to be stably positioned within the same functional pocket (Figs. 7A–7D). Glabridin forms multiple proximity-based contacts ranging from approximately 4.5 to 10.1 Å (Asp623: 5.8 Å, Asn691: 8.8 Å, and Ser759: 9.2 Å) within the RdRp NTP-binding pocket, demonstrating a stable binding pose. Although glabridin lacks triphosphate-mediated electrostatic coordination and the binding affinity shows −6.3 kcal·mol^{-1} compared to RTP (−7.6 kcal·mol^{-1}), it maintains reasonable pocket occupancy, suggesting competitive binding potential. Data suggest that glabridin possesses structural stability at the NTP binding site of SARS-CoV-2 RdRp as an RdRp inhibitor.

Cinnamic aldehyde was reported to inhibit the binding to RBD to hACE2 [18], and we consistently showed that cinnamic aldehyde is an antiviral component of CC, which has been shown to inhibit viral attachment (Figs. 4C and 5D). So, we additionally evaluated the binding affinity of cinnamic aldehyde to the SARS-CoV-2 Spike RBD and hACE2 interface (Figs. 7E and 7F). Molecular docking of cinnamic aldehyde to the RBD-ACE2 interface generated 20 binding poses, and the best binding affinity was −5.4 kcal·mol^{-1}. The best-ranked pose exhibited a 90% interface contact ratio, indicating that 9 out of 10 ligand atoms were positioned within 4 Å of the RBD-hACE2 interface. The interface occlusion analysis revealed that it blocked 12.6% of the total interface (30 out of 238 atoms), supporting a direct inhibitory effect on RBD–hACE2 complex formation. Analysis of critical RBD–ACE2 interactions demonstrated that cinnamic aldehyde disrupted three key interaction pairs (Lys31–Gln493, Glu35–Gln493, and Lys353–Gly502). These data demonstrate that cinnamic aldehyde effectively binds to the RBD–ACE2 interface and directly disrupts interactions essential for viral entry.

3.6. IFN-related antiviral gene induction by MHT via the STAT1 signal pathway

To determine the effect of MHT on the host antiviral response, the expression of IFN-related antiviral genes, including *IFNA1*, *IFNB1*, *IFNL1*, and *MX1,* in virus-infected MRC-5 cells was analyzed. At 1–4 dpi, MHT dose-dependently induced the expression of IFN-related antiviral genes in the absence of HCoV-OC43 infection (Fig. 8A). MHT treatment also resulted in an additive enhancement of the expression levels of these antiviral genes induced by HCoV-OC43 (Fig. 8B).

Since STAT1 mediates the IFN signaling pathway, we analyzed the expression levels of total STAT1 and phospho-STAT1 in MHT-treated MRC-5 cells (Figs. 8C and 8D). Following a 30-min treatment of MHT in MRC-5 cells, an increased expression level of phospho-STAT1 was observed. Additionally, HCoV-OC43 infection itself induced STAT1 phosphorylation for 30 min, and MHT treatment further dose-dependently increased the expression level of phospho-STAT1 during infection. These results suggest that MHT can induce IFN-related antiviral genes, such as *IFNA1*,

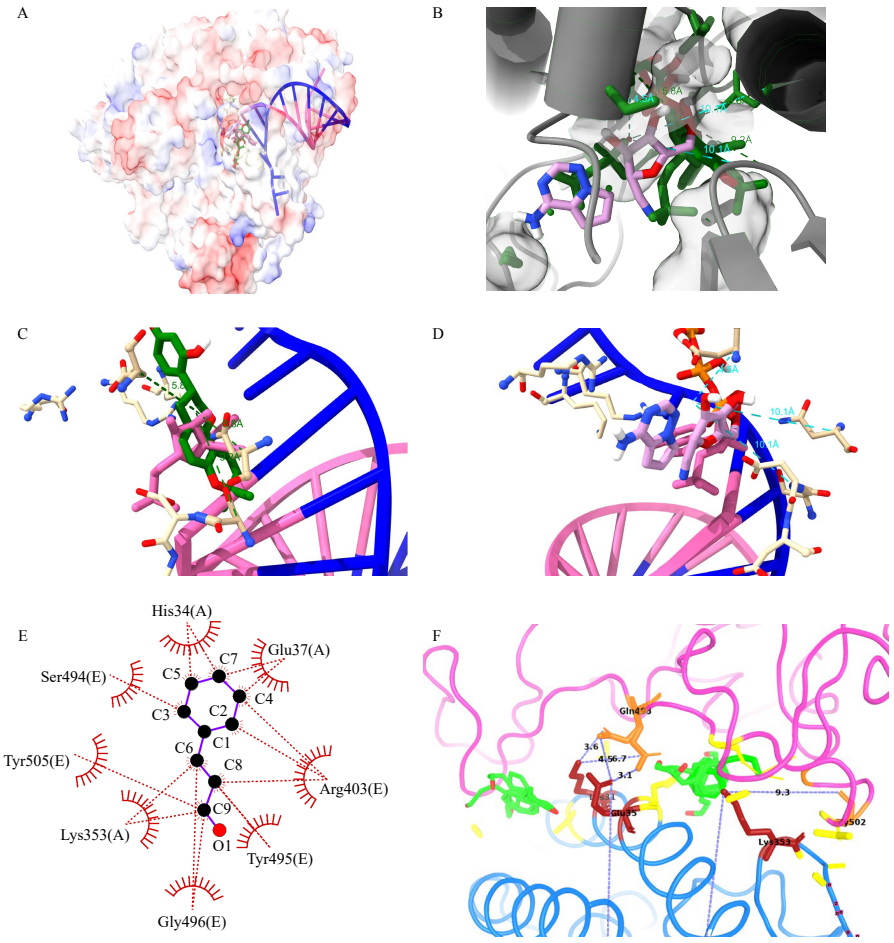


Fig. 7 Molecular docking analysis. (A) Overall structure of SARS-CoV-2 RNA-dependent RNA polymerase (RdRp) highlighting the NTP-binding pocket. Glabridin (green) and the RNA duplex (in blue/pink) are displayed. (B) Close-up view of the experimentally validated NTP-binding site defined by Asp623, Asn691, and Ser759, showing docking poses of remdesivir triphosphate (RTP, orange) and glabridin (green). (C and D) Docking pose and interaction fingerprint of glabridin (C) and RTP (D). (E) 2D interaction diagram of cinnamic aldehyde at the RBD-hACE2 interface. Hydrogen bonds are shown as dashed lines with distances. Hydrophobic contacts are indicated by arc patterns. (F) Disruption of critical RBD (pink)-hACE2 (blue) interactions by cinnamic aldehyde (green). ACE2 residues (Lys31, Glu35, and Lys353) (red), RBD residues (Gln493 and Gly502) (orange). Dashed lines with distance labels indicate disrupted hydrogen bond pairs.

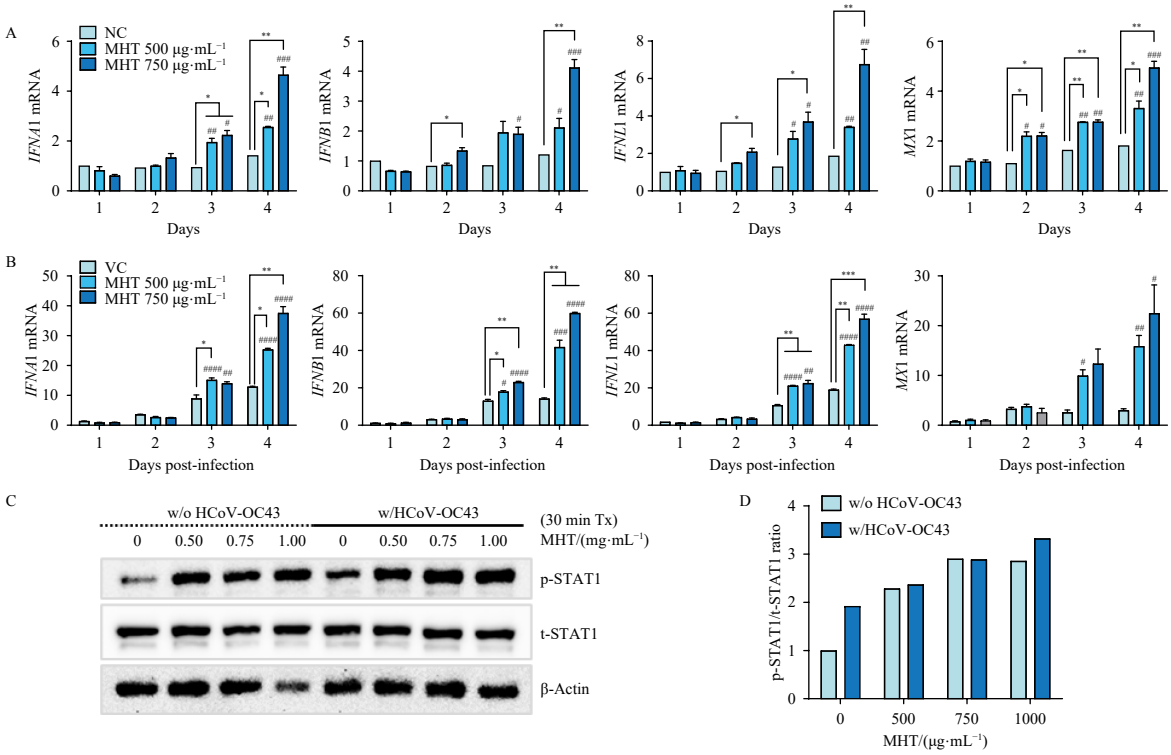


Fig. 8 MHT induced the expression of antiviral interferon (IFN)-related genes *via* the STAT1 signaling pathway. (A) *IFNA1*, *IFNB1*, *IFNL1*, and *MX1* mRNA levels were quantified under MHT treatment using qRT-PCR at 1–4 days. (B) *IFNA1*, *IFNB1*, *IFNL*, and *MX1* mRNA levels were quantified under MHT treatment during HCoV-OC43 infection using qRT-PCR at 1–4 dpi. Data were normalized to the beta-actin (*ACTB*) expression level. Data were analyzed using one-way ANOVA, followed by Bonferroni's multiple comparisons test (*$P < 0.05$, **$P < 0.01$ and ***$P < 0.001$ *vs* NC or VC at the same day; $^{\#}P < 0.05$, $^{\#\#}P < 0.01$, $^{\#\#\#}P < 0.001$ and $^{\#\#\#\#}P < 0.0001$ *vs* mRNA level at Day 1). (C) Expression levels of total STAT1 (t-STAT1) and phosphorylation of STAT1 (p-STAT1) by western blot analysis. (D) The ratio of p-STAT1 to t-STAT1 expression level. β-Actin was used as a control. It was representative of two independent experiments.

IFNB1, *IFNL1,* and *MX1 via* the induction of STAT1 phosphorylation.

4. Discussion

Traditional oriental medicines based on multicomponent and multitarget approaches have garnered attention as potential strategies to enhance the synergistic effects of drugs and reduce toxicities or side effects [19]. These combinations can be analyzed from the perspectives of complementary action, neutralization, facilitation, and pharmacokinetic potentiation [20]. Following the "Kun-Shin-Choa-Sa" (Emperor-Minister-Assistant-Messenger) theory of the MHT formula, ES plays a key role in the primary efficacy of MHT. ES, as the "emperor", disperses qi, induces sweating, and alleviates dyspnea. CC, as the "minister," warms meridians and assists in ES action. PA, as the "assistant," lowers the lung's *qi* (Fèi qì, a pathological condition in which the lung function is oppressed by infections from external pathogens, then the flow of qi is forced upward) and assists ES and CC actions. GU, as the "messenger," moderates the strong effects of the other herbs and harmonizes the formula. The combination of these four herbs in MHT ultimately induces sweating and disperses lung qi, effectively addressing symptoms such as aversion to cold, body aches, cough, and dyspnea. Consequently, MHT has been widely utilized for treating colds, influenza, bronchitis, asthma, and other respiratory conditions. This study explored the inhibitory effect of MHT on human coronavirus infection against HCoV-OC43, SARS-CoV-2, and its variants. We defined the anticoronaviral activity of MHT by targeting the multistep process, the virus entry, the activity of viral proteins (e.g., Mpro, PLpro, and RdRp), and the induction of antiviral cytokines, type I and III IFNs. This comprehensive analysis also uncovered the role of antiviral herbal components and their compounds (Fig. 9).

MHT antiviral activity has been reported. MHT inhibited influenza virus infection in the entry step by blocking endosome acidification [7] and suppressed respiratory syncytial virus attachment to the cell surface by specific interactions with the central conserved domain of the G protein, obstructing viral attachment to the cellular receptor CX3CR1 [21]. We also discovered that MHT inhibited the entry of coronavirus with virucidal activity in a time-of-addition assay, as well as in viral attachment, penetration, and virucidal assays, and a pseudotyped virus infection assay. The variable inhibition rates of SARS-CoV-2 variants and pseudotyped virus infection by MHT could be driven by the structural evolution of the virus, particularly in the spike protein, which is the main target of MHT during viral entry. In the time-of-addition assay, the pre-treatment and post-treatment of MHT showed different effects on HCoV-OC43 and SARS-CoV-2. This apparent discrepancy could be driven by the differences in virus replication kinetics, cell systems, and/or experimental methods. Nevertheless, the optimal working time of MHT was during co-treatment, which is consistent with the experimental data for both HCoV-OC43 and SARS-CoV-2. Among MHT herbal components, CC also exhibited cell-protective effects in the early stage of coronavirus infection. Its main compounds, cinnamic aldehyde, not cinnamic acid, markedly reduced the viral RNA levels. An *in silico* study demonstrated that cinnamic aldehyde can effectively bind to the RBD-hACE2 interface and disrupt critical interactions essential for viral entry. Cinnamic aldehyde could also inhibit the activity of Mpro and PLpro of SARS-CoV-2 in this study. Cinnamic aldehyde demonstrated antiviral effects against the influenza virus *in vitro* and in *vivo*, Herpes Simplex virus type 1, and Respiratory Syncytial virus as a potent antiviral compound [22-25].

Post-treatment with MHT inhibited viral infection, indicating that MHT affected SARS-CoV-2 infection even after viral entry. Notably, the GU component mainly acted in the late stages of the viral life cycle. Based on these findings, we examined the effect of MHT and its components on the activity of viral proteins—Mpro,

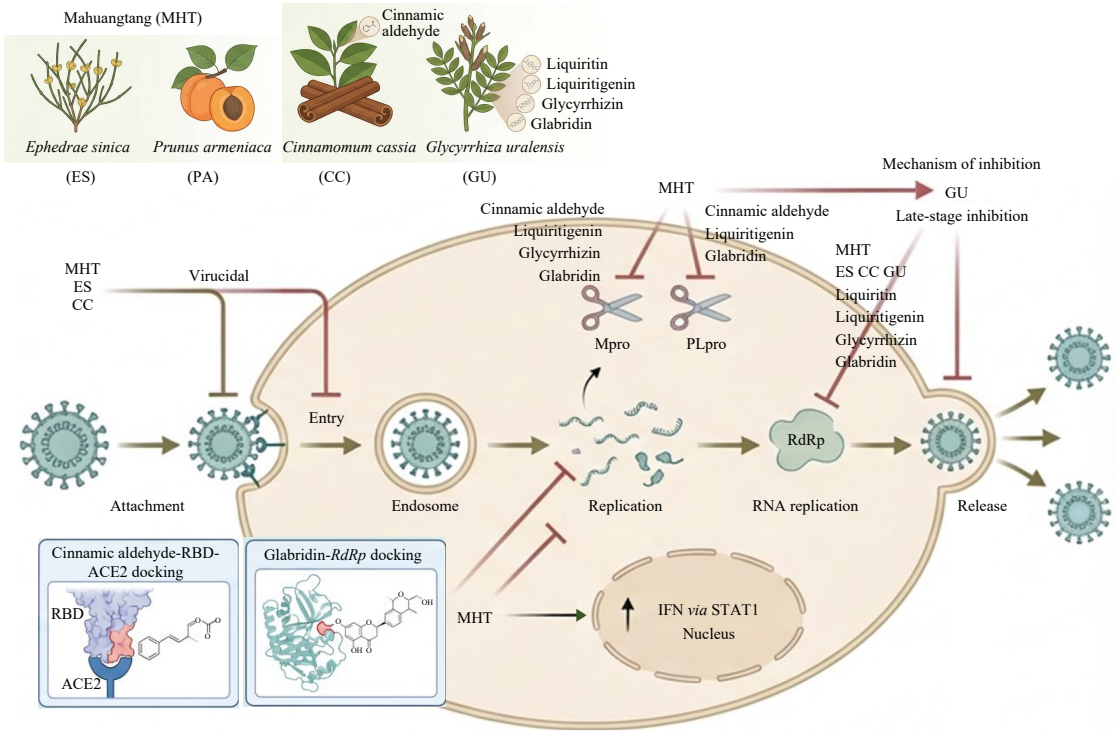


Fig. 9 Schematic representation of the inhibitory mechanism of coronavirus infection by Mahuangtang (MHT).

PLpro, and RdRp—essential for viral replication. We found that MHT and, in particular, GU components, liquiritigenin and glabridin, inhibited Mpro and PLpro proteases activities. In the RdRp activity assay, MHT inhibited RdRp activity, and GU showed the strongest inhibitory activity among MHT components. Compounds in GU (glycyrrhizin, liquiritin, liquiritigenin, and glabridin) showed inhibitory activity on RdRp. The most potent compound, glabridin, possesses structural stability capable of substantially competing with RTP at the NTP binding site of SARS-CoV-2 RdRp in the constraint-based docking analysis. We also verified that the bioactive compounds of GU, liquiritin, liquiritigenin, glycyrrhizin, and glabridin exhibited antiviral activity against HCoV-OC43 by reducing viral copy numbers. Notably, GU and its glycyrrhizin exhibit potent antiviral activity against various viruses, including hepatitis A, B, and C, HIV, Coxsackie, influenza viruses, and SARS-CoV [26, 27], and have been considered as a traditional medicine for alleviating the COVID-19 symptoms [28].

Although ES showed antiviral activity against HCoV-OC43 and SARS-CoV-2, its main compounds in our experiment, L-ephedrine and D-pseudoephedrine, with the pharmacological effects on the cardiovascular and respiratory system [29], could not inhibit coronavirus infection. This finding corroborated a previous report in which ephedrine alkaloid-free ephedra herb extract maintained a comparable level of anti-influenza and SARS-CoV-2 efficacy to ES [30, 31]. Furthermore, *Ephedra przewalskii* extract lacking ephedrine alkaloids exhibited higher antiviral activity against SARS-CoV-2 than ES [32]. These data suggest that ephedrine alkaloids are not responsible for ES antiviral activity. PA and its glycoside derivative, amygdalin, did not show anticoronaviral activity in our study. However, PA has traditionally been employed to alleviate asthma and coughs. Additionally, it showcases diverse pharmacological activities, including antioxidant and anti-inflammatory activities, along with protecting the respiratory, digestive, cardiovascular, and neural systems despite the toxic property of amygdalin [33, 34]. Therefore, PA would be beneficial for COVID-19 treatment.

Virus-infected cells recognize viruses *via* pattern recognition receptors and produce type I and III IFNs as the primary antiviral components contributing to the overall defense mechanism of host cells against viruses [35, 36]. When type I IFNs bind to the IFNα/β receptor, the Janus kinase-STAT pathway is activated, and the expression of IFN-stimulated genes is upregulated [37, 38]. We found that MHT itself induced the expression of IFN-related antiviral genes, including *IFNA1*, *IFNB1*, *IFNL1*, and *MX1 via* STAT1 signaling pathway activation, which were markedly upregulated during virus infection. Therefore, MHT could enhance innate immunity as a type I and III IFN inducer by stimulating the STAT1 signaling pathway, as well as direct-acting antivirals. The post-treatment with MHT inhibited viral infection, suggesting that MHT still inhibited the SARS-CoV-2 infection after viral entry.

5. Conclusion

The traditional herbal formula, MHT, has been widely utilized for treating cold, influenza, and respiratory disease. To analyze the antiviral effects and the mode of action of MHT on human coronavirus infection, HCoV-OC43 and SARS-CoV-2, including omicron variants, were examined. We revealed that MHT exhibited the inhibition of virus entry, induced the expression of IFN-related antiviral genes, and inhibited the activity of the main viral proteins, Mpro, PLpro, and RdRp in the virus life cycle. Moreover, cinnamic aldehyde, liquiritin, liquiritigenin, glycyrrhizin, and glabridin were the active compounds among the nine compounds identified in MHT. Therefore, MHT could be considered as a potential therapeutic agent for treating broad-spectrum coronavirus infectious diseases by targeting the multistep process of infection. Further *in vivo* research and clinical trials are warranted to explore the therapeutic efficacy of MHT.

Funding

This work was supported by grants of the Korea Health Technology R&D Project through the Korea Health Industry Development Institute (KHIDI), funded by the Ministry of Health & Welfare, Republic of Korea (No. RS-2023-KH134941) and the Korea Institute of Oriental Medicine, Republic of Korea (No. KSN2125220).

Supplementary data

Data will be available on request by sending E-mail to the corresponding authors.

Declaration of competing interest

These authors have no conflict of interest to declare.

References

1 V'Kovski P, Kratzel A, Steiner S, et al. Coronavirus biology and replication: implications for SARS-CoV-2. *Nat Rev Microbiol*. 2021;19(3):155-170. https://doi.org/10.1038/s41579-020-00468-6.

2 Ao DY, He XM, Liu J, et al. Strategies for the development and approval of COVID-19 vaccines and therapeutics in the post-pandemic period. *Signal Transduct Target Ther*. 2023;8(1):466. https://doi.org/10.1038/s41392-023-01724-w.

3 Feikin DR, Abu-Raddad LJ, Andrews N, et al. Assessing vaccine effectiveness against severe COVID-19 disease caused by omicron variant. *Report from a meeting of the World Health Organization. Vaccine*. 2022;40(26):3516-3527. https://doi.org/10.1016/j.vaccine.2022.04.069.

4 Yao Y, Zhang XD, Wang ZZ, et al. Deciphering the combination principles of traditional Chinese medicine from a systems pharmacology perspective based on Ma-huang Decoction. *J Ethnopharmacol*. 2013;150(2):619-638. https://doi.org/10.1016/j.jep.2013.09.018.

5 He Y, Gai YQ, Wu XB, et al. Quantitatively analyze composition principle of Ma Huang Tang by structural equation modeling. *J Ethnopharmacol*. 2012;143(3):851-858. https://doi.org/10.1016/j.jep.2012.08.010.

6 Nagai T, Kataoka E, Aoki Y, et al. Alleviative effects of a Kampo (a Japanese herbal) medicine "Maoto (Ma-Huang-Tang)" on the early phase of influenza virus infection and its possible mode of action. *Evid-Based Compl Alt*. 2014;2014:187036. https://doi.org/10.1155/2014/187036.

7 Masui S, Nabeshima S, Ajisaka K, et al. Maoto, a traditional Japanese herbal medicine, inhibits uncoating of influenza virus. *Evid-Based Compl Alt*. 2017;2017:1062065. https://doi.org/10.1155/2017/1062065.

8 Nishi A, Kaifuchi N, Shimobori C, et al. Effects of maoto (ma-huang-tang) on host lipid mediator and transcriptome signature in influenza virus infection. *Sci Rep*. 2021;11(1):4232. https://doi.org/10.1038/s41598-021-82707-1.

9 Wei WY, Wan HT, Peng XQ, et al. Antiviral effects of Ma Huang Tang against H1N1 influenza virus infection *in vitro* and in an ICR pneumonia mouse model. *Biomed Pharmacother*. 2018;102:1161-1175. https://doi.org/10.1016/j.biopha.2018.03.161.

10 Ma CH, Ma ZQ, Fu Q, et al. Ma Huang Tang ameliorates asthma though modulation of Th1/Th2 cytokines and inhibition of Th17 cells in ovalbumin-sensitized mice. *Chin J Nat Med*. 2014;12(5):361-366. https://doi.org/10.1016/S1875-5364(14)60044-3.

11 Yoshino T, Arita R, Horiba Y, et al. The use of maoto (Ma-Huang-Tang), a traditional Japanese Kampo medicine, to alleviate flu symptoms: a systematic review and meta-analysis. *BMC Complem Altern Med*. 2019;19(1):68. https://doi.org/10.1016/j.heares.2006.09.015.

12 Kubo T, Nishimura H. Antipyretic effect of Mao-to, a Japanese herbal medicine, for treatment of type A influenza infection in children. *Phytomedicine*. 2007;14(2–3):96-101. https://doi.org/10.1016/J.PHYMED.2006.09.015.

13 Kim DE, Min JS, Jang MS, et al. Natural bis-benzylisoquinoline alkaloids-tetrandrine, fangchinoline, and cepharanthine, inhibit human Coronavirus OC43 infection of MRC-5 human lung cells. *Biomolecules*. 2019;9(11):696. https://doi.org/10.3390/biom9110696.

14 Kim JM, Chung YS, Jo HJ, et al. Identification of Coronavirus isolated from a patient in Korea with COVID-19. *Osong Public Health Res Perspect*. 2020;11(1):3-7. https://doi.org/10.24171/j.phrp.2020.11.1.02.

15 Habib M, Jin YH, Kim Y, et al. Anticoronavirus activity of rhizome of *Dryopteris crassirhizoma via* multistage targeting of virus entry and viral proteases, Mpro and PLpro. *J Ethnopharmacol*. 2024;333:118490. https://doi.org/10.1016/j.jep.2024.118490.

16 Min JS, Kwon S, Jin YH. SARS-CoV-2 RdRp inhibitors selected from a cell-based SARS-CoV-2 RdRp activity assay system. *Biomedicines*. 2021;9(8):996. https://doi.org/10.3390/biomedicines9080996.

17 Trott O, Olson AJ. AutoDock Vina: improving the speed and accuracy of docking with a new scoring function, efficient optimization, and multithreading. *J Comput Chem*. 2010;31(2):455-461. https://doi.org/10.1002/jcc.21334.

18 Nishimura Y, Nomiyama K, Okamoto S, et al. Identification of anti-SARS-CoV-2 agents based on flavor/fragrance compositions that inhibit the interaction between the virus receptor binding domain and human angiotensin converting enzyme 2. *PLoS One*. 2022;17(12):e0279182. https://doi.org/10.1371/journal.pone.0279182.

19 Luo GA, Wang YM, Liang QL, et al. *Systems Biology for Traditional Chinese Medicine*. John Wiley & Sons, 2012. https://doi.org/10.1002/9781118313367.

20 Kim HU, Ryu JY, Lee JO, et al. A systems approach to traditional oriental medicine. *Nat Biotechnol*. 2015;33(3):264-268. https://doi.org/10.1038/nbt.3167.

21 Fujikane A, Sakamoto A, Fujikane R, et al. *Ephedrae* herba and *Cinnamomi* cortex interactions with G glycoprotein inhibit respiratory syncytial virus infectivity. *Commun Biol*. 2022;5(1):94. https://doi.org/10.1038/s42003-022-03046-z.

22 Liu R, Ting HE, Zeng N, et al. Mechanism of anti-influenza virus of volatile oil in Cinnamomi Ramulus and cinnamaldehyde. *Chin Tradit Herb Drugs*. 2013;44(11):1460-1464. https://doi.org/10.7501/j.issn.0253-2670.2013.11.019.

23 Zhou J, Yuan XR, Li L, et al. Comparison of different methods for extraction of *Cinnamomi ramulus*: yield, chemical composition and *in vitro* antiviral activities. *Nat Prod Res*. 2017;31(24):2909-2913. https://doi.org/10.1080/14786419.2017.1299724.

24 Hayashi K, Imanishi N, Kashiwayama Y, et al. Inhibitory effect of cinnamaldehyde, derived from *Cinnamomi* cortex, on the growth of influenza A/PR/8 virus *in vitro* and *in vivo*. *Antiviral Res*. 2007;74(1):1-8. https://doi.org/10.1016/j.antiviral.2007.01.003.

25 Liu J, Zhang Q, Li RL, et al. The traditional uses, phytochemistry, pharmacology and toxicology of *Cinnamomi ramulus*: a review. *J Pharm Pharmacol*. 2020;72(3):319-342. https://doi.org/10.1111/jphp.13189.

26 Wang LQ, Yang R, Yuan BC, et al. The antiviral and antimicrobial activities of licorice, a widely-used Chinese herb. *Acta Pharm Sin B*. 2015;5(4):310-315. https://doi.org/10.1016/j.apsb.2015.05.005.

27 Sun ZG, Zhao TT, Lu N, et al. Research progress of glycyrrhizic acid on antiviral activity. *Mini Rev Med Chem*. 2019;19(10):826-832. https://doi.org/10.2174/1389557519666190119111125.

28 Banerjee S, Baidya SK, Adhikari N, et al. Glycyrrhizin as a promising kryptonite against SARS-CoV-2: clinical, experimental, and theoretical evidences. *J Mol Struct*. 2023;1275:134642. https://doi.org/10.1016/j.molstruc.2022.134642.

29 Drew CD, Knight GT, Hughes DT, et al. Comparison of the effects of D-(−)-ephedrine and L-(+)-pseudoephedrine on the cardiovascular and respiratory systems in man. *Br J Clin Pharmacol*. 1978;6(3):221-225.

30 Hyuga S, Hyuga M, Oshima N, et al. Ephedrine alkaloids-free *Ephedra* herb extract: a safer alternative to ephedra with comparable analgesic, anticancer, and anti-influenza activities. *J Nat Med*. 2016;70(3):571-583. https://doi.org/10.1007/s11418-016-0979-z.

31 Uema M, Hyuga M, Yonemitsu K, et al. Antiviral effect of ephedrine alkaloids-free *Ephedra* herb extract against SARS-CoV-2 *in vitro*. *Microorganisms*. 2023;11(2):534. https://doi.org/10.3390/microorganisms11020534.

32 Kakimoto M, Nomura T, Nazmul T, et al. *In vitro* anti-severe acute respiratory syndrome coronavirus 2 effect of *Ephedra przewalskii* Stapf extract. *J Ethnopharmacol*. 2024;319(Pt 3):117341. https://doi.org/10.1016/j.jep.2023.117341.

33 Tang S, Wang MM, Peng YH, et al. Armeniacae semen amarum: a review on its botany, phytochemistry, pharmacology, clinical application, toxicology and pharmacokinetics. *Front Pharmacol*. 2024;15:1290888. https://doi.org/10.3389/fphar.2024.1290888.

34 Wei YM, Li YN, Wang SG, et al. Phytochemistry and pharmacology of Armeniacae Semen Amarum: a review. *J Ethnopharmacol*. 2023;308:116265. https://doi.org/10.1016/j.jep.2023.116265.

35 Samuel CE. Interferon at the crossroads of SARS-CoV-2 infection and COVID-19 disease. *J Biol Chem*. 2023;299(8):104960. https://doi.org/10.1016/j.jbc.2023.104960.

36 Diamond MS, Kanneganti TD. Innate immunity: the first line of defense against SARS-CoV-2. *Nat Immunol*. 2022;23(2):165-176. https://doi.org/10.1038/s41590-021-01091-0.

37 Kawai T, Akira S. Innate immune recognition of viral infection. *Nat Immunol*. 2006;7(2):131-137. https://doi.org/10.1038/ni1303.

38 Platanias LC. Mechanisms of type-I- and type-II-interferon-mediated signalling. *Nat Rev Immunol*. 2005;5(5):375-386. https://doi.org/10.1038/nri1604.